Transient Pressure Analysis of Volume Fracturing Well in Fractured Tight Oil Reservoirs

Cheng Lu[1, 2], Jiahang Wang[2], Cong Zhang[1, 2], Minhua Cheng[3], Xiaodong Wang[2], Wenxiu Dong[2], Yingfang Zhou[4*]

([1].The Key Laboratory of Unconventional Petroleum Geology, CGS, Beijing 100029, China; [2]. China University of Geosciences, Beijing 100083; [3]. Research Institute of Petroleum Exploration& Development, Beijing 100083; [4] School of Engineering, University of Aberdeen, Aberdeen AB24 3UE. * Corresponding author.)

Abstract：This paper presents a semi-analytical model to simulate transient pressure curves for vertical well with reconstructed fracture network in fractured tight oil reservoirs. In the proposed model, the reservoir is a composite system and contains two regions. The inner region is described as formation with finite conductivity hydraulic fracture network and the flow in the fracture is assumed to be linear; while the outer region is modeled using the classical Warren-Root model and where radial flow is applied. The transient pressure curves of a vertical well in the proposed reservoir model are calculated semi-analytically using Laplace transform and Stehfest numerical inversion. As shown in the type curves, the flow is divided into several regimes: (a) linear flow in artificial main fractures; (b) coupled boundary flow; (c) early linear flow in fractured formation; (d) mid radial flow in the semi-fractures of the formation; (e) mid radial flow or pseudo steady flow; (f) mid cross-flow (g) closed boundary flow. Based on our newly proposed model, the effects of some sensitive parameters, such as elastic storativity ratio, cross-flow coefficient, fracture conductivity and skin factor on the type curves were also analyzed extensively. The simulated type curves shows that for vertical fractured well in tight reservoir the elastic storativity ratios and crossflow coefficients affect the time and degree of crossflow respectively. The pressure loss increases with the increase of fracture conductivity. To a certain extent, the effect of fracture conductivity is more obvious than that of the half length of the fracture on improving production effect. With the increase of wellbore storage coefficient, fluid compressibility is so big that might cover the early stage characteristic of fracturing. Linear or bilinear flow may not be able to see, the pressure and pressure derivative gradually shifted to the right. With the increase of skin effect, the pressure loss

increases gradually.

Keywords: well test analysis, fractured tight oil reservoir, fracture network reconstruction, composite system

1. Introduction

The development of tight oil reservoirs has been attracting increasing attentions in China. Hydraulic fracturing treatments are considered as the primary effective stimulation approach of boosting the productivity of wells producing from these low permeability reservoirs. During the last few decades, there has been a continuous increasing interest in the determination of formation properties from transient pressure test or flow rate data analysis [1-7]. However, the conventional fracturing of a single fracture cannot meet the needs of industrial production, and the single fracture model couldn't represent the complicated hydraulic fractures in real reservoir conditions.

Volume fracturing technique is one of these methods that have been widely applied to improve the productivity of low permeability tight reservoirs. After repeatedly acid fracturing treatment to fracture failure brittle reservoirs, hydraulic fracture, natural fracture and shear cracks are mutually staggered and thus form a certain stimulated zone of joint fracture network near the wellbore, which then changes the flow pattern, reduce the flow resistance, improve production of single well [8-11]. Test and evaluate fracture network reconstruction along the well and its pressure behavior are essential for improving the performance of production well in tight reservoirs after stimulation treatment. Transient pressure analyzing is one of the key methodologies to estimate reservoir parameters, such as permeability, porosity, length, widths and skin factor.

The behavior of transient pressure curve in fractured well has been attracted increasing attention recently because of the advanced techniques in fracturing. In terms of numerical simulation, Khalid established the model by using the vertical and horizontal orthogonal crack network to approximate substitute volume reconstruction [12], and this model has been widely used since then [13-15]. Arvind combined the micro

seismic exploration results to fit the volume and the degree of the transformation region to approximate the micro fracture network around wells [17]. However, Chang describes the transformation region volume by using the Kazemi dual medium mode [18]. In terms of the analytic model, Liu and Zhao [19-20] and Lei and Gang [21] described the fracture distribution of volume transformation region of vertical wells by using the fractal theory, and the production of cold and heavy oil with carrying sand is studied based on their model. Recently, composite reservoir model with permeability and fractal dimension was applied to evaluate the productivity of tight oil reservoir [22-23].

Compared with the analytical methods, the numerical simulation methods are capable to deal with the complicated seepage problem to a large extent by the grid division, while the procedure is complicated and will require amount of computation resources. The fractal theory can describe the spatial distribution of fracture better, but it does not apply to the pressure transmission behavior and the artificial fracture parameter optimization research. Liao and Chen described the pressure transient analysis of volume fracturing well without considering the wellbore storage effect and skin effect, and five flow regimes were recognized in their simulated transient pressure type curves [24].

As mentioned above, the transient pressure behavior for the vertical wells with stimulated volume in fractured tight reservoirs is not addressed properly as appeared in the literature. In this work, we proposed a semi-analytical model to simulate the transient pressure curves of stimulated vertical well in fractured tight reservoir by Laplace transform and Stehfest numerical inversion [25]. This is accomplished by representing micro fractures produced by the volume fracturing as the dual medium model, and coupling with the formation of micro fractures by discretizing the artificial fracture. The semi-analytical solution that describes pressure transient behavior of volume fracturing in fractured tight reservoir is obtained and then applied to investigate the impact of fracture conductivity ratio, coefficient of pressure, storage capacity ratio and flow coefficient on type curves and flow regimes.

2. Mathematical Model

A stimulated volume with joint network is formed near the wellbore in brittle tight reservoirs after repeatedly acid fracturing treatments. The stimulated fracture network normally could be subdivided into two parts, the inner artificial main fracture and the outer classic natural fractured zone, respectively. The fluid flow in the main fracture is linear and follows the Darcy's law, and the fracture conductivity is subjected to change other than infinite simplification. While the classical Warren-Root model [26] is used to describe the fracture distribution and seepage flow in the outer area, in this region there is no artificial fractures and thus the permeability is very low (< 0.1mD) because of low connectivity. Affected by the extension of the artificial fracture and the brittle shear of reservoir rock in outer area, the artificial fracture and natural fracture are arranged in a crisscross pattern and thus changes the flow pattern mainly to fracture. In this work, the fluid supplied to the stimulated volume region by natural fractures is neglected since it is much smaller comparing with that from the artificial main fracture [27-28]. In summary, the model assumptions are listed below:

(1) The reservoir is homogeneous and isotropic along the radial direction.

(2) The production is constant, fluid and rock are micro compressible.

(3) Fractures are the main flow channels, the seepage flow is laminar and isothermal.

(4) The conductivity of vertical artificial fracture is finite and the fracture is fully penetrating the formation with the height equal to the thickness of the reservoir.

A well with stimulated reservoir volume (SRV) locates in a circular closed reservoir. The main vertical fracture has a finite conductivity and with a half-length x_f, a width b_f, a permeability k_f, and fully penetrates the formation vertically. The classical Warren-Root model is used to simulate the micro fractures produced by the stimulated reservoir volume in the reservoir formation. The reservoir is composed of a fracture network and matrix blocks. The fracture network possesses a bulk fracture porosity ϕ_{2f}

and total compressibility c_{2f}. The matrix blocks are slabs of thickness h, permeability k_{2m}, porosity ϕ_{2m} and total compressibility c_{2m}.

The reservoir contains a fluid of viscosity μ which is slightly compressible. The flow process in the system under consideration can be studied by breaking up the medium into three parts and taking the interaction among the different parts into account. These regions are: hydraulic fracture in the inner area, reservoir fracture network and reservoir matrix in the outer area (see in Fig. 1).

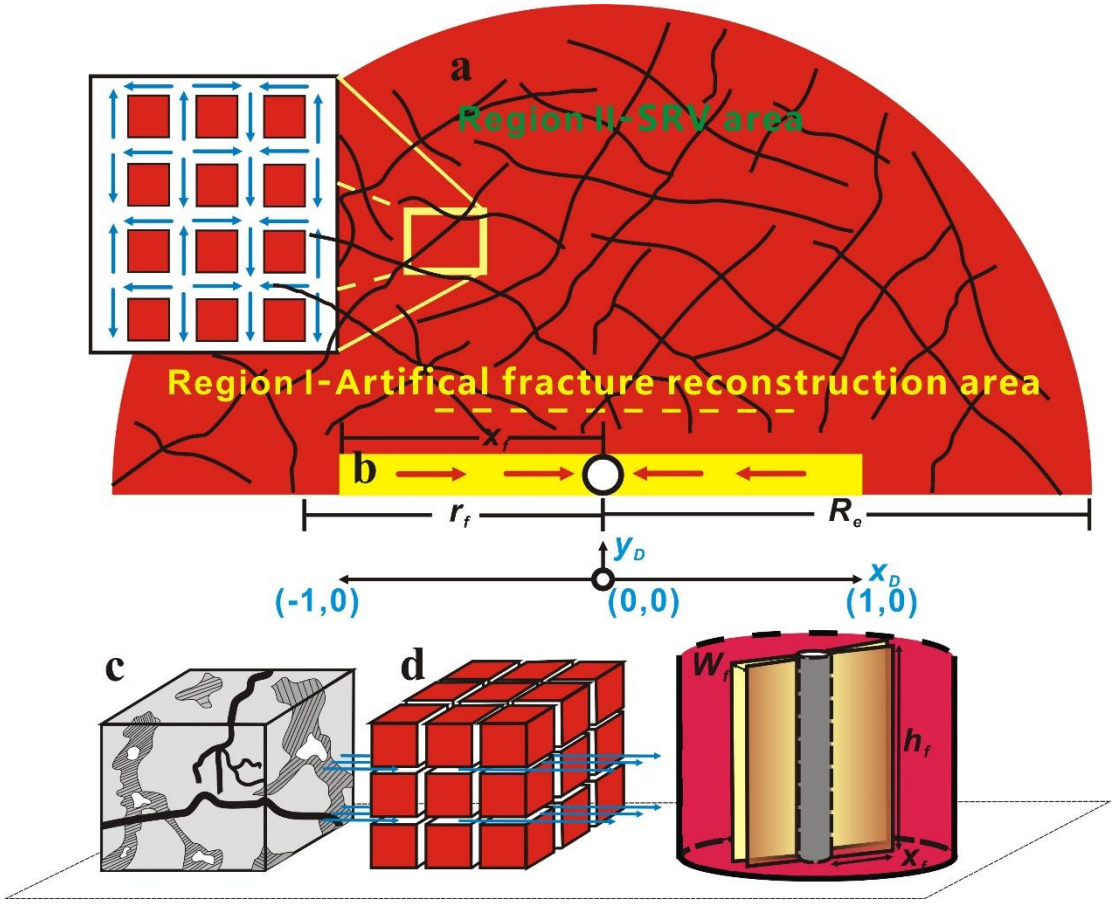

Fig.1 Schematic diagram: **a**. stimulated reservoir volume model. **b** physical modeling scheme of artificial main fracture. **c** the system of matrix. **d** classic Warren-root dual medium model

2.1. Fluid flow in the main vertical fracture

The flow within the hydraulic fracture is considered as linear because the fracture width, b_f, is much smaller than fracture length and fracture height. It is assumed that flow into the wellbore takes place only through the hydraulic fracture; and flow from the

reservoir into the hydraulic fracture occurs only through the reservoir fracture network because k_{2f} is much larger than k_{2m}. In addition, no flow is allowed into the fracture through the fracture tips. Fig.1 illustrates the characteristic of this model; here $q_f(x,t)$ is the flow rate going to the fracture per unit of length.

Cinco-Ley and Samaniego has demonstrated that the compressibility of the hydraulic fracture can be neglected for practical purposes because the fracture volume is very limited [29]. Hence the flow within the fracture can be considered as incompressible. Under these conditions, the transient flow in the hydraulic fracture can be described by the following equations in terms of dimensionless variables

$$\frac{\partial^2 p_{fD}}{\partial x_D^2}+\frac{2}{c_{fD}}\frac{\partial p_{2fD}(y_D,t_D)}{\partial y_D}=0\,,0<x_D<1 \tag{1}$$

Inner boundary condition

$$\frac{dp_{fD}(0)}{dx_D}=-\frac{\pi}{c_{fD}} \tag{2}$$

Outer boundary condition

$$\frac{dp_{fD}(1)}{dx_D}=0 \tag{3}$$

The flow correlation formula for surface of the fracture

$$q_{fD}=-\frac{2}{\pi}\frac{\partial p_D}{\partial y_D}\bigg|_{y_D=\frac{w_{fD}}{2}} \tag{4}$$

We can obtain solutions in Laplace domain through combining the Eqs.(1)-(4), that is

$$p_{wD}(x_D)-p_{fD}(x_D)=\frac{\pi}{c_{fD}}\left(x_D-\int_0^{x_D}\int_0^{v}q_{fD}(u,t_D)dudv\right) \tag{5}$$

Where

$$P_{nD}=\frac{k_{2f}h(P_i-P)}{1.842\times10^{-3}q\mu B},n=f,f2,m2,$$

$$w_D=\frac{w_f}{x_f}\quad,\quad x_D=\frac{x}{x_f}\quad,\quad y_D=\frac{y}{x_f}\quad,\quad c_{fD}=\frac{k_f w_f}{k_{2f}x_f}\quad,\quad t_{D\omega}=\frac{3.6\eta_\omega t}{x_f^2}\quad,$$

$$\eta_\omega=\frac{k_{2f}}{\mu(\phi_{2f}c_{2f}+\phi_{2m}c_{2m})},$$

$$\omega_2 = \frac{(\phi c)_{2f}}{(\phi c)_{2f} + (\phi c)_{2m}},$$

$$\lambda_2 = \frac{\gamma k_{2m} x_f^2}{k_{2f}}$$

2.2. Fluid flow in micro fractures

As mentioned above, the formation is stimulated reservoir volume which is full of micro fractures. The reservoir is represented by a fracture network and matrix blocks. It is assumed that the characteristics of both the fracture network and matrix blocks remain constant within the reservoir. The flow from the reservoir into the hydraulic fracture occurs through the fracture network only, as generally considered in the literatures for double porosity reservoirs.

The transient flow in the formation can be described by

$$\frac{\partial^2 \tilde{p}_{2fD}}{\partial r_D^2} + \frac{1}{r_D}\frac{\partial \tilde{p}_{2fD}}{\partial r_D} = s\tilde{p}_{2fD} - \tilde{q}_{2mD} \tag{6}$$

Because $q = -(V\phi c_t)_{2m}\frac{\partial P_{2m}}{\partial t} = \frac{k_{2m}A_{2m}}{\mu l V}(P_{2m} - P_{2f}) = \frac{k_{2m}}{\mu l^2}(P_{2m} - P_{2f})$ (7)

We can get the equation below

$$q_{2mD} = \lambda_2 (P_{2fD} - P_{2mD}) = (1-\omega_2)\frac{\partial P_{2mD}}{\partial t_{D\omega}} \tag{8}$$

The Eq. (6) can be further simplified

$$\frac{\partial^2 \tilde{p}_{2fD}}{\partial r_D^2} + \frac{1}{r_D}\frac{\partial \tilde{p}_{2fD}}{\partial r_D} = sf_2(s)\tilde{p}_{2fD} \tag{9}$$

Inner boundary condition

$$\left[r_D \frac{\partial \tilde{P}_{2fD}}{\partial r_D} \right]_{r_D=0} = -\frac{q_f}{q} = -\tilde{q}_{fD} \tag{10}$$

Outer boundary condition

$$\left[r_D \frac{\partial \tilde{P}_{2fD}}{\partial r_D} \right]_{r_D = r_{eD}} = 0 \tag{11}$$

Where

$$f_2(s) = \frac{\omega_2(1-\omega_2)s + \lambda_2}{(1-\omega_2)s + \lambda_2}$$

Combining Eq. (6)-(11) can obtain formation transient flow point source solution

$$\tilde{p}_{2fD} = \tilde{q}_{fD}(s) \cdot \left[\frac{K_1\left(r_{eD}\sqrt{z}\right)}{I_1\left(r_{eD}\sqrt{z}\right)} I_0\left(r_D\sqrt{z}\right) + K_0\left(r_D\sqrt{z}\right) \right] \tag{12}$$

Where

$$z = s\frac{\omega_2(1-\omega_2)s + \lambda_2}{(1-\omega_2)s + \lambda_2} = sf_2(s)$$

Further, the solution of plane source is obtained by integrating point source in term of Bessel functions. The pressure distribution of this system is then given by

$$\tilde{p}_{2fD}(x_D, 0, s) = \frac{1}{2}\int_{-1}^{1} \tilde{q}_{fD} \left[\frac{K_1\left(r_{eD}\sqrt{z}\right)}{I_1\left(r_{eD}\sqrt{z}\right)} I_0\left\{\left[(x_D-\sigma)^2\right]^{1/2}\sqrt{z}\right\} + K_0\left\{\left[(x_D-\sigma)^2\right]^{1/2}\sqrt{z}\right\} \right] d\sigma \tag{13}$$

Combining Eq. (5) and (13) results in

$$\begin{aligned} \tilde{p}_{wD}(s) &= \frac{\pi}{sc_{fD}} \left(x_D - s\int_0^{x_D}\int_0^{v} \tilde{q}_{fD}(u)\,du\,dv \right) \\ &+ \frac{1}{2}\int_{-1}^{1} \tilde{q}_{fD} \left[\frac{K_1\left(r_{eD}\sqrt{z}\right)}{I_1\left(r_{eD}\sqrt{z}\right)} I_0\left\{\left[(x_D-\sigma)^2\right]^{1/2}\sqrt{z}\right\} + K_0\left\{\left[(x_D-\sigma)^2\right]^{1/2}\sqrt{z}\right\} \right] d\sigma \end{aligned} \tag{14}$$

Considering the fracture symmetry

$$\tilde{q}_{fD}(\sigma, s) = \tilde{q}_{fD}(-\sigma, s) \tag{15}$$

Eq. (14) becomes

$$\begin{aligned} &\tilde{p}_{wD}(s) - \frac{\pi}{sc_{fD}} \left(x_D - s\int_0^{x_D}\int_0^{v} \tilde{q}_{fD}(u)\,du\,dv \right) = \\ &\frac{1}{2}\int_0^1 \tilde{q}_{fD} \left[\frac{K_1\left(r_{eD}\sqrt{z}\right)}{I_1\left(r_{eD}\sqrt{z}\right)} \left\{ I_0\left((x-\sigma)\sqrt{z}\right) + I_0\left((x+\sigma)\sqrt{z}\right) \right\} + \left\{ K_0\left((x-\sigma)\sqrt{z}\right) + K_0\left((x+\sigma)\sqrt{z}\right) \right\} \right] d\sigma \end{aligned} \tag{16}$$

Eq. (16) gives the transient solution in vertical fracture with finite conductivity of

stimulated reservoir volume.

3. Solution and Validation

The wellbore pressure of a constant production hydraulic fracturing well in naturally fractured reservoirs is estimated by solving Eq. (16) semi-analytical of the following matrix using a Gaussian elimination approach, and the detailed derivation of Eq. (A20) is presented as an appendix.

$$\begin{bmatrix} W(1,1) & W(1,2) & W(1,3) & W(1,4) & W(1,5) & \cdots & W(1,50) & 1 \\ \cdots & \cdots & \cdots & \cdots & \cdots & \cdots & \cdots & 1 \\ W(50,1) & W(50,2) & W(50,3) & W(50,4) & W(50,5) & \cdots & W(50,50) & 1 \\ 1 & 1 & 1 & 1 & 1 & \cdots & 1 & 0 \end{bmatrix} \begin{bmatrix} \tilde{q}_{fD1} \\ \cdots \\ \tilde{q}_{fD50} \\ \tilde{p}_{wD} \end{bmatrix} = \begin{bmatrix} \frac{\pi x_{D1}}{sc_{fD}} \\ \cdots \\ \frac{\pi x_{D50}}{sc_{fD}} \\ \frac{1}{s\Delta x} \end{bmatrix} \quad \text{(A20)}$$

Riley gave an analytical solution for elliptical finite conductivity fractures without volume fracturing [30]. To validate the solution presented in this paper, we compared our solution with Riley's results. In our model, elastic storativity ratio ω and crossflow coefficient λ are considered to be equal to one, and skin factor *S* are considered to be equal to zero, which is under the same assumption for Riley's results. Fig.2 shows the comparison of the two solutions under different fracture conductivity C_{fD}, the good agreement validates the solution obtained in this work.

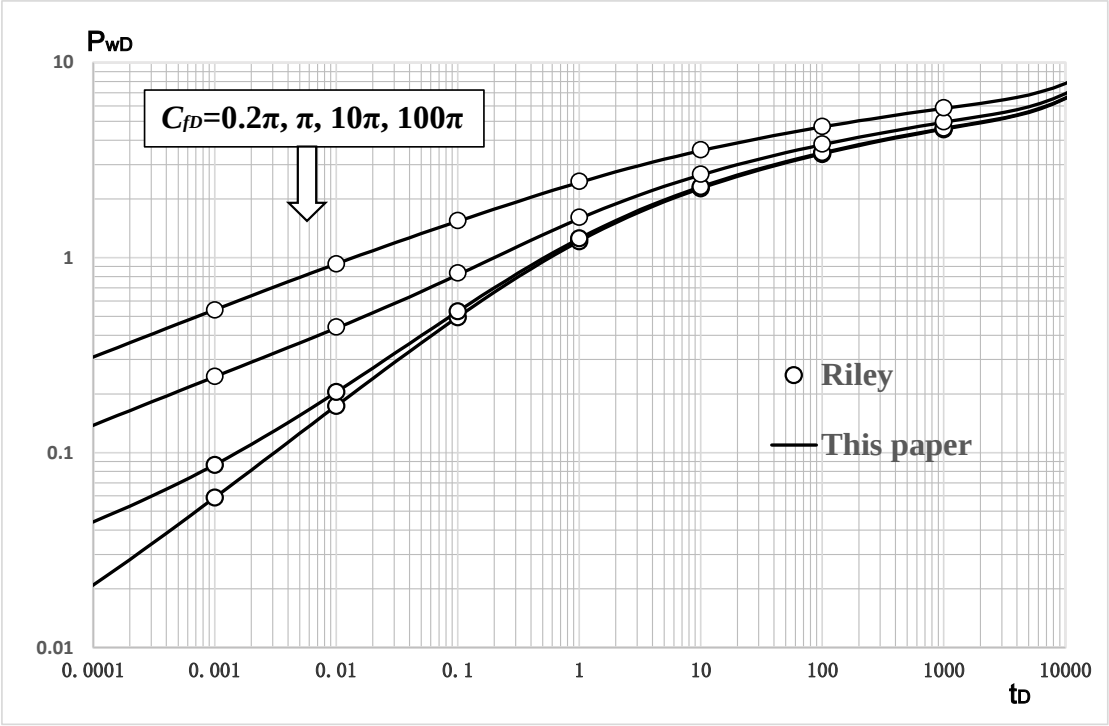

Fig.2 The comparison for the results of this paper and Riley (1991)

3.1. Flow Regimes

The pressure and its derivative curves are presented in Fig. 3, which shows basic flow characteristics for a SRV well in fractured reservoir with different parameters by using stehfest numerical inversion. The parameters are given as: c_{fD}=0.1，ω=0.00001，λ=0.01; c_{fD}=1，ω=0.01，λ=0.01; c_{fD}=10（infinite boundary），ω=0.005，λ=0.0001; c_{fD}=100，ω=0.01，λ=0.0001; c_{fD}=300，ω=0.01，λ=0.0001. As shown in Fig. 2, the flow can be divided into 7 stages, and they are described below.

A. Early bilinear flow regime (artificial fracture and fractured reservoirs near the wellbore):

In this stage, the segment has a straight line with slope equals to 1/4, demonstrating the bilinear flow region (see Fig.3). In this region, fluids flow through fracture to wellbore, and from reservoirs to fracture at the same time. This region could be identified only if the fracture conductivity is relatively small.

B. Early coupled boundary flow regime:

In this stage, the reservoir stimulated volume is fractured and modified well, and thus the artificial main fracture conductivity is much larger than that of the double medium fracture system. The fluid in the artificial main fracture reaches wellbore rapidly; however, the double medium fracture system cannot provide adequate fluid supply. Both pressure and pressure derivate curves increases, similar to the transient pressure response of weak energy supply or closed boundary reservoir.

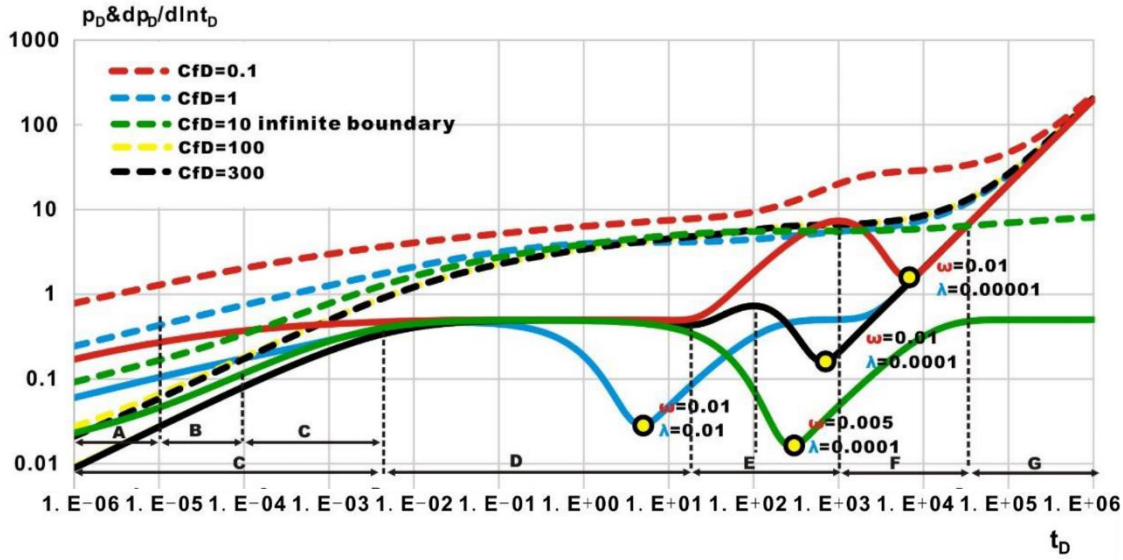

(a)

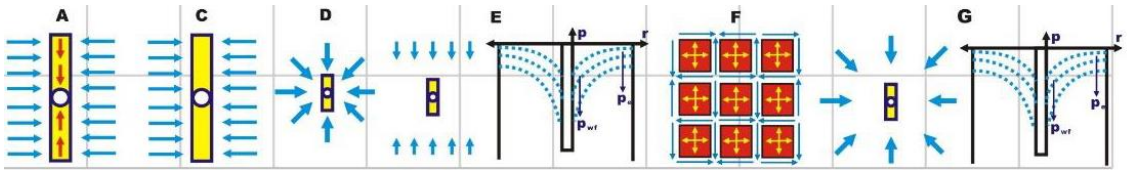

(b)

Fig.3 Flow stage division

C. Early linear flow (fractured reservoir near the wellbore):

The pressure and pressure derivative curves are both straight lines with slope equal to 1/2, which clearly demonstrates early linear flow. In this region, fluid flow linearly directly from formation to the artificial fracture, this is optimal flow mode because it reduces the seepage resistance. The early A and B flow regions do not necessarily occur for each fracturing treatment, which depends on the conductivity of artificial fracture flow. As shown in Fig. 3, the bilinear flow is more obviously for the case with smaller fracture conductivity.

D. Middle radial flow (micro fractures in the fractured formation):

The segment has a straight line with 0.5 constant, namely, mid radial flow.

E. Middle bilinear flow or pseudo steady state flow:

The larger the cross-flow factor λ is, the earlier the time of fluid channeling occurs. Before fluid crossflow between microcracks and formation occurs it will exhibit pseudo steady flow or mid linear flow briefly which is affected by the cross-flow coefficient λ. Specifically, if λ is small it will exhibit pseudo steady flow when the pressure reach the boundary or linear flow when the pressure wave disturbance does not reach the boundary.

F. Middle crossflow (matrix and fracture)：

Because the permeability of matrix is very low and thus the pressure drop is extremely slow, so crossflow occur between the matrix and fracture. And the pressure derivative curve is concave. Compared to the conventional dual media the time of channeling is much earlier. At the same time, due to the dimensionless setting cross-flow coefficient λ is 2 to 4 orders of magnitude larger than that of the conventional dual medium.

G. Late pseudo steady flow：

For infinite outer boundary, the pressure derivative curve is a horizontal line. While for closed outer boundary, the slope of pressure and pressure derivative cures is 1. In some cases affected by the elastic storativity ratio ω and crossflow coefficient λ the medium segment has different flow characteristics: D+E or D+F.

3.2. Influencing Factors on Wellbore Pressure

3.2.1. Elastic storativity ratio *w* and crossflow coefficient λ

The dimensionless pressure and pressure derivative of different elastic storativity ratios (ω=0.01, 0.05, 0.1, 0.5, 1) and different crossflow coefficients (λ=1×10^{-5}，1×10^{-4}，1×10^{-3}，1×10^{-2}) is given in the Fig.4 and Fig.5, respectively.

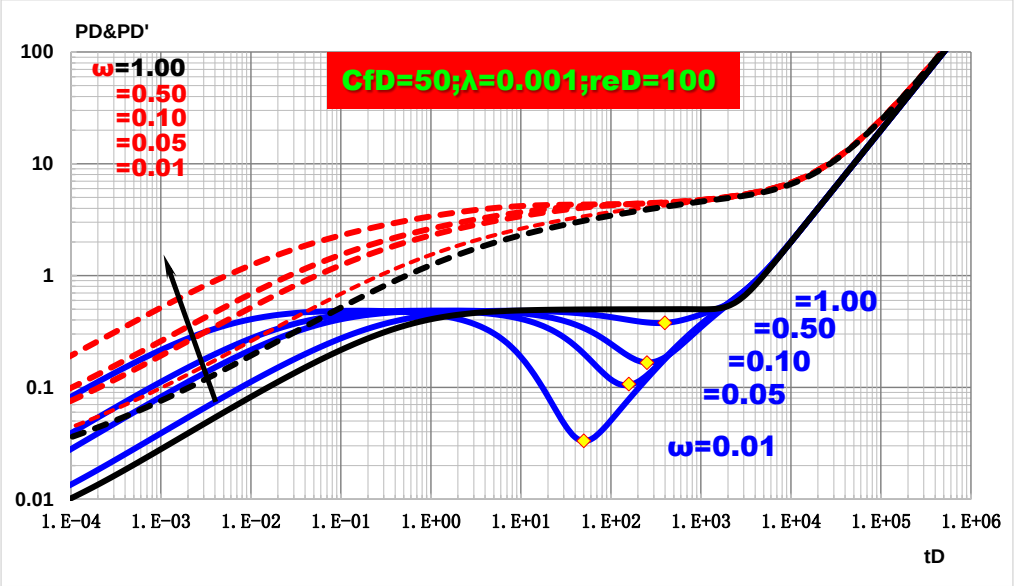

Fig.4 The effect of elastic storativity ratio factor on type curves

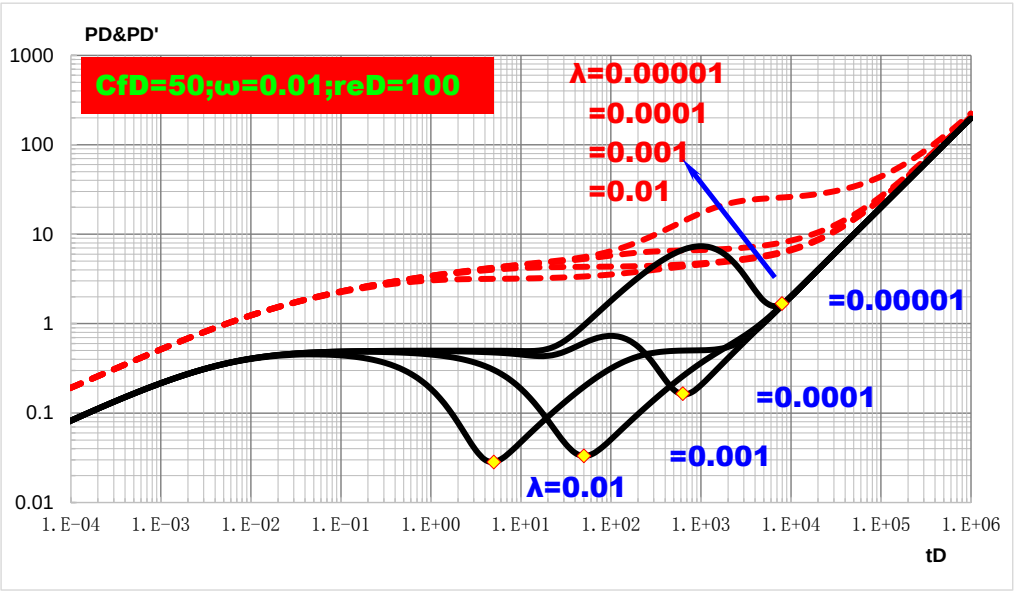

Fig.5 The effect of crossflow coefficient factor on type curves

From these two figures, we can see that similar to the common dual media elastic storativity ratios and different crossflow coefficients affect the time and degree of crossflow, respectively. The elastic storativity ω ratio has an influence on the production of transitional flow. The smaller the elastic storativity ω is, the more obvious the crossflow is. At the intermediate time, curve of pressure derivative is sunken. The larger the elastic storativity ω is, the smaller the peak value of pressure derivative is. The crossflow coefficient λ ratio has an influence on the cross flow between matrix-fracture. The bigger the interporosity flow coefficient is, the earlier

the interporosity flow happens. Fig 5 shows that if the cross flow coefficient is relatively small and the pressure wave does not touch the boundary, the medium linear flow could be recognized; and after the pressure wave reaching the boundary, pseudo steady flow occurs.

3.2.2. Fracture conductivity C_{fD}

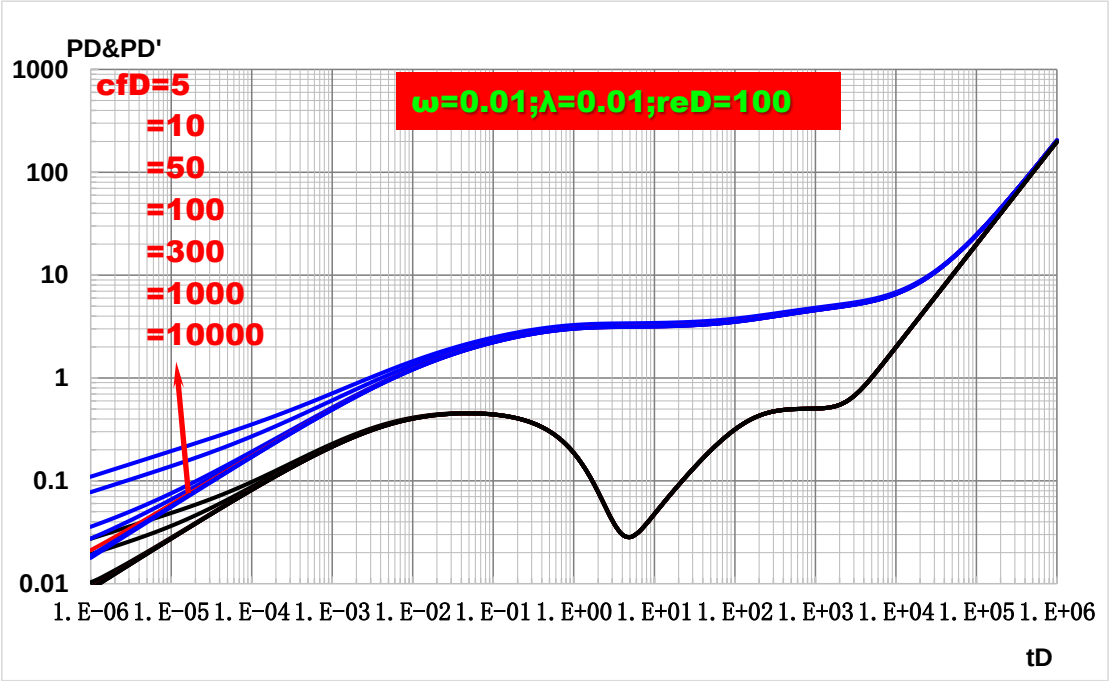

Fig.6 The effect of fracture conductivity factor on type curves

The result of artificial fracturing is to leave a high permeability channel in the near well formation, which is convenient for the fluid to flow from the well zone to the bottom hole or for the injection agent from the bottom hole to the reservoir. In Fig.6, the dimensionless artificial fracture conductivity ranges from 5 to 10000. The pressure loss increases with the increase of fracture conductivity and the range of the pressure drop funnel becomes larger especially in the effective SRV region. To a certain extent, the effect of fracture conductivity is much more significant than that of the half length of the fracture for improving production. Fracture conductivity is actually determined by the fracture permeability and width of fracture. The fact of fracture conductivity is the quality of fluid from reservoir to fracture per unit pressure gradient. While for constant production well it is reflected by the unit production of the pressure loss.

3.2.3. Wellbore storage effect and skin effect

The effect of skin and wellbore storage on the transient pressure curves primary reflected in the early stage. The slope of the pressure and pressure derivative is 1 on the double logarithmic curve. With the increase of wellbore storage coefficient, fluid compressibility is so big that it might cover the early stage characteristic of fracturing. Linear or bilinear flow may not be able to recognized, the pressure and pressure derivative gradually shifted to the right. With the increase of skin effect, the pressure derivative increases gradually. When the skin effect is too large, the pressure derivative has great value, which indicates that the well fracturing is not successful.

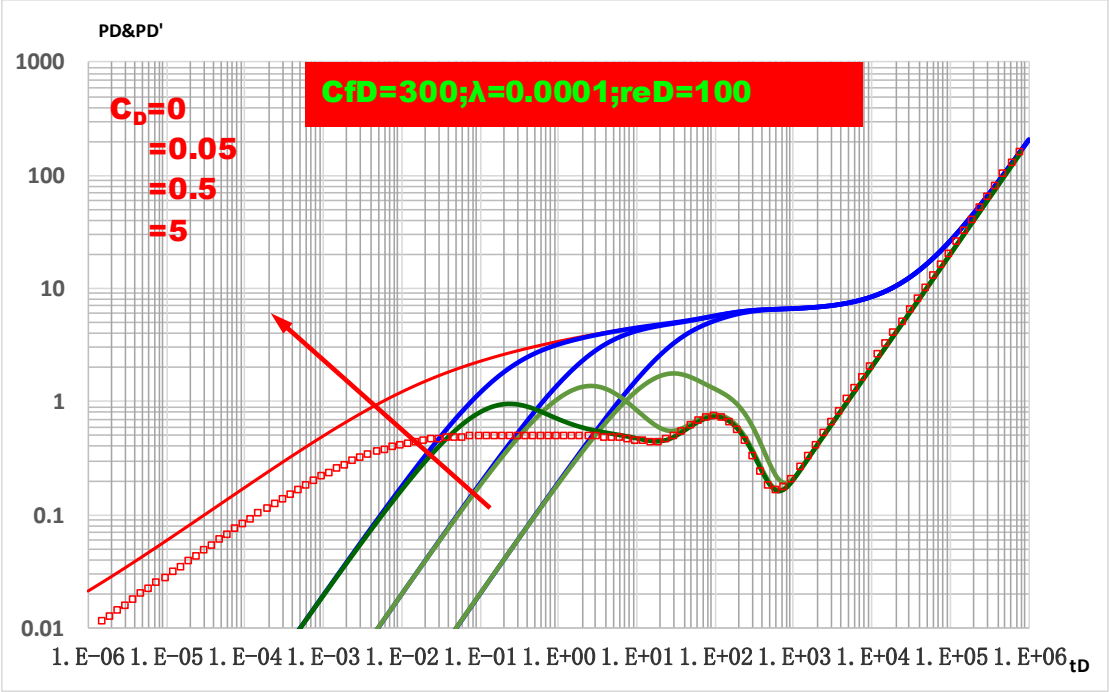

Fig.7 The effect of wellbore storage factor on type curves

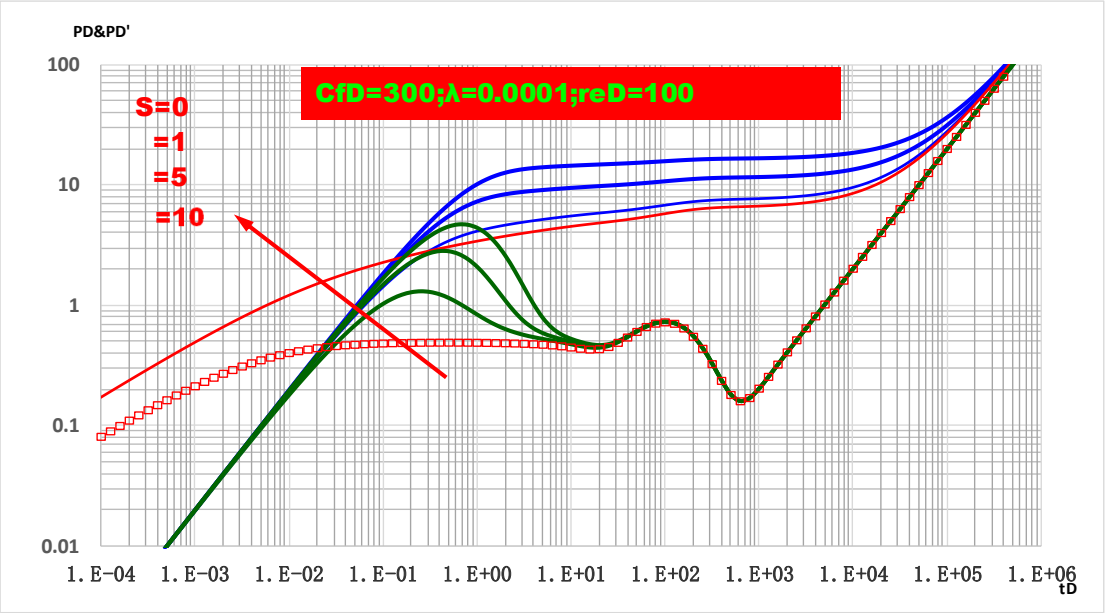

Fig.8 The effect of skin factor on type curves

4. Conclusions

In this study, we have investigated the transient pressure characteristics of transient pressure analysis of volume fracturing vertical well in fractured tight oil reservoir. The specific conclusions are

(1) Using Laplace transform and Stehfest numerical inversion method, a semi-analytical model to simulate transient pressure curves for vertical well with reconstructed fracture network is established in fractured tight oil. The effect of an artificial main fracture near wellbore is also took into account in this model and it can simply reflect the flow characteristics of the production wells in each stage after fracturing and acidizing treatment. This model is suitable for the reconstruction of multiple fracturing of vertical wells in fractured reservoirs with closed boundary and the evaluation of vertical well volume stimulation in fractured tight reservoirs.

(2) Based on the established models, new type curves are established to analyze the flow characteristics, which can be divided into seven stages: (a) linear flow in artificial main fractures; (b) coupled boundary flow; (c) early linear flow in

fractured formation; (d) mid radial flow in the semi-fractures of the formation; (e) mid radial flow or pseudo steady flow; (f) mid cross-flow and (g) closed boundary flow.

(3) Effects of some sensitive parameters, such as elastic storativity ratio, cross-flow coefficient, fracture conductivity, wellbore storage effect and skin effect, on type curves were analyzed in details. Elastic storativity ratios and crossflow coefficients affect the time and degree of crossflow respectively. Artificial fracturing can leave a high permeability channel in the near well formation, which is convenient for the fluid to flow from the well zone to the bottom hole or the injection agent from the bottom hole to the formation. The pressure loss increases with the increase of fracture conductivity. To a certain extent, the effect of fracture conductivity is more obvious than that of the half length of the fracture on improving production effect. With the increase of wellbore storage coefficient, fluid compressibility is so big that might cover the early stage characteristic of fracturing. Linear or bilinear flow may not be able to see, the pressure and pressure derivative gradually shifted to the right. With the increase of skin effect, the pressure loss increases gradually.

Nomenclature

Dimensionless Variables: Real Domain

C_{fD} = dimensionless artificial main fracture conductivity

p_{wD} = dimensionless well bottom pressure

p_{2fD} = dimensionless micro fracture pressure in volume modification region

p_{fD} = dimensionless artificial main fracture pressure

t_D = dimensionless time

x_{Di} = midpoint of the i segment

γ = Euler constant, 05771

Dimensionless Variables: Laplace Domain

$\widetilde{p}_D$ = the pressure p_D in Laplace domain

$\widetilde{p}_{wD}$ = the pressure p_{wD} in Laplace domain

$\widetilde{p}_{2fD}$ = dimensionless micro fracture pressure p_{2fD} in Laplace domain

$\widetilde{p}_{fD}$ = artificial main fracture pressure p_{fD} in volume modification region in Laplace domain

s = time variable in Laplace domain, dimensionless

Field Variables

A = reservoir drainage area, m^2

c_{2m} = compressibility for matrix, 1/Mpa

c_{2f} = compressibility for micro fracture, 1/Mpa

ϕ_{2m} = porosity for matrix, fraction

ϕ_{2f} = porosity for micro fracture

k_f = permeability of artificial main fracture, mD

k_{2f} = permeability of micro fracture, mD

k_{2m} = permeability of matrix, mD

p = formation pressure, Mpa

p_i = initial formation pressure, Mpa

r = reservoir radius, m

r_e = equivalent drainage radius, m

t =time variable, days

x_f = fracture half-length, m

w = fracture width, m

ω_2 = elastic storativity ratio ratio, fraction

λ_2 = crossflow coefficient, fraction

Special Functions

$K_0(x)$= Modified Bessel function (2nd kind, zero order)

$K_1(x)$= Modified Bessel function (2nd kind, first order)

$I_0(x)$= Modified Bessel function (1st kind, zero order)

$I_1(x)$= Modified Bessel function (1st kind, first order)

Special Subscripts

Dd = dimensionless decline variable

i = integral function (or initial value)

id =integral derivative function

pss = pseudo steady-state

Acknowledgements

This research was supported by the Ministry of Land and Resources Special Geological Survey: Upper Paleozoic Marine Shale Gas Geological Survey in Yunnan, Guizhou, Guangxi Region (DD20160178), The Key Laboratory of Unconventional Petroleum Geology of Geological Survey of China Open Fund and the Major National R&D Projects: Study on the Test Method for Shale Structure and Composition at Different Scales with project number: 2016ZX05034-003-006.

References

1. Raghavan, R., Uraiet, A., and Thomas, G. W., 1976, "Vertical Fracture Height: Effect on Transient Flow Behavior," 51th Annual Fall Technical Conference and Exhibition of SPE, New Orleans, Oct. 3-6., Paper No. SPE 6016
2. Cinco-Ley, H., and Samaniego, V. F., 1978, "Effect of Wellbore Storage and Damage on the Transient Pressure Behavior of Vertically Fractured Wells," 52th Annual Fall Technical Conference and Exhibition of the Society of Petroleum Engineers of AIME, Denver, CO, Paper No. SPE 6752
3. Cinco-Ley, H., and Samaniego-V., F., 1981, "Transient Pressure Analysis for Fractured Wells," J. Pet. Technol., 33(9), pp. 1749–1766.
4. Wang, L., Wang, X., 2016. Modelling of pressure transient behaviour for fractured gas wells under stress-sensitive and slippage effects. Int. J. Oil. Gas Coal Technol. 11 (No. 1), 18e38.
5. Xu, W., Wang, X., Hou, X., et al. 2016. Transient analysis for fractured gas wells by modified pseudofunctions in stress-sensitive reservoirs. Journal of Natural Gas Science and Engineering 35: 1129-1138.
6. Wei, M., Duan, Y., Dong, M. and Fang, Q., 2016. Blasingame decline type curves with material balance pseudo-time modified for multifractured horizontal wells in shale gas reservoirs. J. Nat. Gas Sci. Eng. 31 340–50.
7. Wei, M., Duan, Y., Fang, Q. and Zhang, T., 2016. Production decline analysis for a multi-fractured horizontal well considering elliptical reservoir stimulated volumes in shale gas reservoirs. J. Geophys. Eng. 13 (2016) 354–365.
8. Jia C., Zou C., Li J., and et al, 2012. Assessment criteria, main types, basic features and resource prospects of the tight oil in China. Acta Petrolei Sinica, 33(3), 343-350, May.
9. Zou C., Zhu R., Wu S., and et al, 2012. Types, characteristics, genesis and prospects of conventional and unconventional hydrocarbon accumulations: taking tight oil and tight gas in China as an instance. Acta Petrolei Sinica, 33(2), 173-187, March.
10. Nan J., Wang S., Yao W., and et al, 2007. Micro-fractures in extra-low permeability reservoir of Yanchang Formation in Ordos Basin. Lithologic Reservoir, 19(4), 40-44, December.
11. Guo Y., Liu J., Yang H., et al, 2012. Hydrocarbon accumulation mechanism of low permeable tight lithologic oil reservoirs in the Yanchang Formation, Ordos Basin, China. Petroleum Exploration and Development, 39(4), 417-425, August.
12. Khalid M., Mansour A., 2009. Tight Oil Reservoir Development Feasibility Study Using Finite Difference Simulation and Streamlines. Paper SPE 126099 presented at the 2009 SPE Saudi Arabia Section Technical Symposium and Exhibition held in AIKhobar, Saudi Arabia, 09-11 May.
13. Cipolla C.L., Carbo C., Lolon E.P., at el, 2009. Reservoir Modeling and Production Evaluation in Shale-Gas Reservoirs, Paper IPTC 13185 presented at the International Petroleum Technology

Conference held in Doha, Qatar, 7-9 December.

14. Barry R., 2010. Accurate simulation of Non-Darcy Flow in Stimulated Fractured Shale Reservoirs. Paper SPE 132093 presented at the SPE Western Regional Meeting held in Anaheim, California, USA, 27-29 May.
15. Wang W., Zhao G., Su Y., and et al, 2013. Application of network fracturing technology to tight oil reservoir. XINJIANG PETROLEUM GEOLOGY, 34(3), 345-348, June.
16. Wang W., Su Y., Mu L., and et al, 2013. Influencing factors of stimulated reservoir volume of vertical wells in tight oil reservoir. Journal of China University of Petroleum, 37(3), 93-97, June.
17. Arvind, H., Franz, D., Martin, C., and at el, 2010. Volumetric Fracture Modeling Approach (VFMA): Incorporating Microseismic Data in the Simulation of Shale Gas Reservoirs. Paper SPE 134683 presented at the SPE Annual Technical Conference and Exhibition held in Florence, Italy, 19-22 September.
18. Chang, M., Xu Z., Lang Z., and at el, 2010. Modeling Hydraulic Fracturing Induced Fracture Networks in Shale Gas Reservoirs as a Dual Porosity System. Paper SPE 132180 presented at the CPS/SPE International Oil& Gas Conference and Exhibition in China held in Beijing, China, 8-10 June.
19. Liu X., Zhao G, 2005. A Fractal Wormhole Model for Cold Heavy Oil Production. Journal of Canadian Petroleum Technology, 44 (9), 31-36, September.
20. Liu X., Zhao G., Jin Y., 2006. Coupled Reservoir/wormholes Model for Cold Heavy Oil Production Wells. Journal of Petroleum Science and Engineering, 50, 258-268.
21. Lei X., Gang Z., 2012. A Novel Approach for determining Wormhole Coverage in CHOPS Wells. Paper SPE 157935 presented at the SPE Heavy Oil Conference Canada held in Calgary, Alberta, Canada, 12-14 June.
22. Liu X., 2013.The Research of Deliverability Evaluated for Volume Reconstruction in Tight oil Reservoir. China University of Geosciences (Beijing).
23. Liu X., Tian C.B., Jiang L.Y., 2014. Steady State Deliverability Evaluation Model of Fracture Network Reconstruction Vertical Well in Tight Oil Reservoir. Journal of Northeast Petroleum University, 38(1), 91-97, February.
24. Liao X. and Chen X., 2016. Pressure transient analysis of volume fracturing well in low permeability oil reservoir. Science & Technology Review, 34(7), 117-122.
25. Stehfest H., 1970. Numerical Inversion of Laplace Transforms. Communications of the ACM, 13(1), 47-49.
26. Warren. J. E and Root, P. J., 1963. The Behavior of Naturally Fractured Reservoirs, Society of Petroleum Engineers Journal, 3(03). DOI, http://dx.doi.org/10.2118/426-PA.
27. Ge J., Ning Z., Liu Y., and et al, 2003. Modern reservoir seepage rule. Petroleum industry Press. 189-194.
28. Medeiros F., Kurtoglu B., Ozkan E., et al, 2007. Pressure-transient performance of hydraulically horizontal well in locally and globally naturally fractured formations. Paper IPTC 11781-MS

presented at the International Petroleum Technology Conference. Dubai, U.A.E., 4-6 December.

29. Cinco L, Samaniego V, Dominguez A, 1978. Transient pressure behavior for a well with a finite-conductivity vertical fracture. Society of Petroleum Engineers Journal, 18(4), 253-264.

30. Riley, M. F., 1991, "Analytical Solutions for Elliptical Finite-Conductivity Fractures," Paper SPE 22656 presented at the 66th Annual Technical Conference and E14. Liu X., Zhao G, 2005. A Fractal Wormhole Model for Cold Heavy Oil Production. Journal of Canadian Petroleum Technology, 44 (9), 31-36, September.

Appendix:

Assuming the fracture can be divided into *n* segments (Fig.A1), the first part on the right side of Eq. (16) could write as

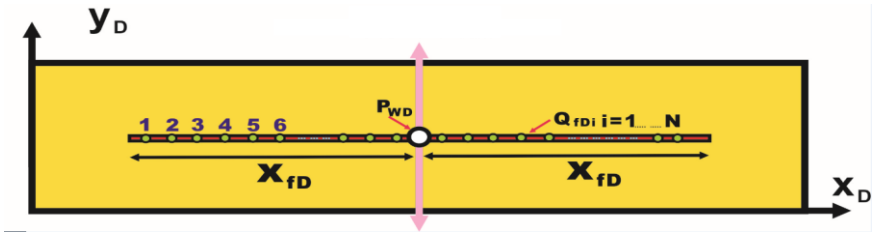

Fig.A1 Schematic diagram of the discrete segment of the fracture

$$\frac{1}{2}\frac{K_1\left(r_{eD}\sqrt{z}\right)}{I_1\left(r_{eD}\sqrt{z}\right)}\int_0^1 \tilde{q}_{fD}\left\{I_0\left((x-\sigma)\sqrt{z}\right)+I_0\left((x+\sigma)\sqrt{z}\right)\right\}d\sigma$$
$$=\frac{1}{2}\frac{K_1\left(r_{eD}\sqrt{z}\right)}{I_1\left(r_{eD}\sqrt{z}\right)}\times\sum_{i=1}^{n}\tilde{q}_{fD}(\sigma,s) \qquad \text{(A1)}$$
$$\int_{x_{Di-1}}^{x_{Di}}\left\{I_0\left((x-\sigma)\sqrt{z}\right)+I_0\left((x+\sigma)\sqrt{z}\right)\right\}d\sigma$$

and the second part can be expressed as

$$\frac{1}{2}\int_0^1 \tilde{q}_{fD}\left\{K_0\left((x-\sigma)\sqrt{z}\right)+K_0\left((x+\sigma)\sqrt{z}\right)\right\}d\sigma$$
$$=\frac{1}{2}\times\sum_{i=1}^{n}\tilde{q}_{fD}(\sigma,s)\int_{x_{Di-1}}^{x_{Di}}\left\{K_0\left((x-\sigma)\sqrt{z}\right)+K_0\left((x+\sigma)\sqrt{z}\right)\right\}d\sigma \qquad \text{(A2)}$$

By using variable substitution method to solve the problem of K_0 and I_0 integral Bessel function as follows

$$\int_{-1}^{1} K_0\left[\sqrt{(x-\alpha)^2}\,\varepsilon_n\right]d\alpha = \frac{1}{\varepsilon_n}\left\{\pi - \left[Ki_1(\varepsilon_n + \varepsilon_n x_D) + Ki_1(\varepsilon_n - \varepsilon_n x_D)\right]\right\} \quad \text{(A3)}$$

$$\int_{-1}^{1} I_0\left[\sqrt{(x-\alpha)^2}\,\varepsilon_n\right]d\alpha = \frac{1}{\varepsilon_n}\left[Ii_1(\varepsilon_n + \varepsilon_n x_D) + Ii_1(\varepsilon_n - \varepsilon_n x_D)\right] \quad \text{(A4)}$$

where

$$Ki_1(x) = \int_x^{\infty} K_0(t)dt$$

$$Ii_1(x) = \int_{\infty}^{x} I_0(t)dt \quad \text{(A5)}$$

1. If ***j*>*i*:**

$$\int_{x_{Di-1}}^{x_{Di}} K_0\left[\left(x_{Dj} - \sigma\right)\sqrt{z}\right]d\sigma = \frac{1}{\sqrt{z}}\left\{Ki_1\left[\left(x_{Dj} - x_{Di}\right)\sqrt{z}\right] - Ki_1\left[\left(x_{Dj} - x_{Di-1}\right)\sqrt{z}\right]\right\} = a(j,i) \quad \text{(A6)}$$

$$\int_{x_{Di-1}}^{x_{Di}} I_0\left[\left(x_{Dj} - \sigma\right)\sqrt{z}\right]d\sigma = \frac{1}{\sqrt{z}}\left\{Ii_1\left[\left(x_{Dj} - x_{Di}\right)\sqrt{z}\right] - Ii_1\left[\left(x_{Dj} - x_{Di-1}\right)\sqrt{z}\right]\right\} = b(j,i) \quad \text{(A7)}$$

2. If ***j*<*i*:**

$$\int_{x_{Di-1}}^{x_{Di}} K_0\left[\left(x_{Dj} - \sigma\right)\sqrt{z}\right]d\sigma = \frac{1}{\sqrt{z}}\left\{Ki_1\left[\left(x_{Di-1} - x_{Dj}\right)\sqrt{z}\right] - Ki_1\left[\left(x_{Di} - x_{Dj}\right)\sqrt{z}\right]\right\} = a(j,i) \quad \text{(A8)}$$

$$\int_{x_{Di-1}}^{x_{Di}} I_0\left[\left(x_{Dj} - \sigma\right)\sqrt{z}\right]d\sigma = \frac{1}{\sqrt{z}}\left\{Ii_1\left[\left(x_{Di-1} - x_{Dj}\right)\sqrt{z}\right] - Ii_1\left[\left(x_{Di} - x_{Dj}\right)\sqrt{z}\right]\right\} = b(j,i) \quad \text{(A9)}$$

3. If ***j*=*i*:**

$$\int_{x_{Di-1}}^{x_{Di}} K_0\left[\left(x_{Dj} - \sigma\right)\sqrt{z}\right]d\sigma = \int_{x_{Di-1}}^{x_{Dj}} K_0\left[\left(x_{Dj} - \sigma\right)\sqrt{z}\right]d\sigma + \int_{x_{Dj}}^{x_{Di}} K_0\left[\left(\sigma - x_{Dj}\right)\sqrt{z}\right]d\sigma = \frac{1}{\sqrt{z}}\left\{\pi - 2Ki_1\left[0.5x_D\sqrt{z}\right]\right\} = a(j,i)$$

$$\int_{x_{Di-1}}^{x_{Di}} I_0\left[\left(x_{Dj} - \sigma\right)\sqrt{z}\right]d\sigma = \int_{x_{Di-1}}^{x_{Dj}} I_0\left[\left(x_{Dj} - \sigma\right)\sqrt{z}\right]d\sigma + \int_{x_{Dj}}^{x_{Di}} I_0\left[\left(\sigma - x_{Dj}\right)\sqrt{z}\right]d\sigma = \frac{2}{\sqrt{z}}\left\{Ii_1\left[0.5x_D\sqrt{z}\right]\right\} = b(j,i)$$

(A10)

4. If ***j*=*i*, *j*<*i*, *j*>*i*:**

$$\int_{x_{Di-1}}^{x_{Di}} K_0\left[\left(x_{Dj} + \sigma\right)\sqrt{z}\right]d\sigma = \frac{1}{\sqrt{z}}\left\{Ki_1\left[\left(x_{Dj} + x_{Di-1}\right)\sqrt{z}\right] - Ki_1\left[\left(x_{Dj} + x_{Di}\right)\sqrt{z}\right]\right\} = c(j,i) \quad \text{(A11)}$$

$$\int_{x_{Di-1}}^{x_{Di}} I_0\left[\left(x_{Dj}+\sigma\right)\sqrt{z}\right]d\sigma=\frac{1}{\sqrt{z}}\left\{Ii_1\left[\left(x_{Dj}+x_{Di-1}\right)\sqrt{z}\right]-Ii_1\left[\left(x_{Dj}+x_{Di}\right)\sqrt{z}\right]\right\}=d(j,i) \tag{A12}$$

And the second-order integral of Eq. (16) can be expressed as

$$\begin{aligned}\int_0^{x_D}\int_0^{v}\tilde{q}_{fD}(u)dudv &= x_{Dj}\int_0^{x_{Dj}}\tilde{q}_{fD}(u,s)du-\int_0^{x_{Dj}}\tilde{q}_{fD}(v,s)vdv \\ &=\sum_{i=1}^{j-1}\tilde{q}_{fDj}\left[\frac{\Delta x_D^2}{2}+\left(x_{Dj}-i\Delta x_D\right)\Delta x_D\right]+\frac{\tilde{q}_{fDj}(s)}{8}\Delta x_D^2\end{aligned} \tag{A13}$$

Assuming,

$$E(j,i)=\frac{1}{2}\left[a(j,i)+c(j,i)\right]+\frac{1}{2}\frac{K_1\left(r_{eD}\sqrt{z}\right)}{I_1\left(r_{eD}\sqrt{z}\right)}\left[b(j,i)+d(j,i)\right] \tag{A14}$$

$$F(j,i)=\int_0^{x_{Dj}}\int_0^{v}\tilde{q}_{fD}(u)dudv=\sum_{i=1}^{j-1}\tilde{q}_{fDj}\left[\frac{\Delta x_D^2}{2}+\left(x_{Dj}-i\Delta x_D\right)\Delta x_D\right]+\frac{\tilde{q}_{fDj}(s)}{8}\Delta x_D^2 \tag{A15}$$

And then

j=1：

$$\tilde{p}_{wD}(s)+\left(\frac{\pi F(1,1)}{c_{fD}}-\frac{E(1,1)}{2}\right)\tilde{q}_{fD1}(s)-\frac{1}{2}\sum_{i=1}^{n}\tilde{q}_{fDi}(s)E(1,i)=\frac{\pi x_{D1}}{sc_{fD}} \tag{A16}$$

j=2：

$$\tilde{p}_{wD}(s)+\left(\frac{\pi F(2,1)}{c_{fD}}-\frac{E(2,1)}{2}\right)\tilde{q}_{fD1}(s)+\left(\frac{\pi F(2,2)}{c_{fD}}-\frac{E(2,2)}{2}\right)\tilde{q}_{fD2}(s)-\frac{1}{2}\sum_{i=1}^{n}\tilde{q}_{fDi}(s)E(2,i)=\frac{\pi x_{D2}}{sc_{fD}} \tag{A17}$$

j=3：

$$\begin{aligned}&\tilde{p}_{wD}(s)+\left(\frac{\pi F(3,1)}{c_{fD}}-\frac{E(3,1)}{2}\right)\tilde{q}_{fD1}(s)+\left(\frac{\pi F(3,2)}{c_{fD}}-\frac{E(3,2)}{2}\right)\tilde{q}_{fD2}(s) \\ &+\left(\frac{\pi F(3,3)}{c_{fD}}-\frac{E(3,3)}{2}\right)\tilde{q}_{fD3}(s)-\frac{1}{2}\sum_{i=1}^{n}\tilde{q}_{fDi}(s)E(3,i)=\frac{\pi x_{D3}}{sc_{fD}}\end{aligned} \tag{A18}$$

.....

j=50

In addition to the above expressions, due to steady flow, we also have

$$\Delta x_D \sum_{i=1}^{50} \tilde{q}_{fDi}(s) = \frac{1}{s} \tag{A19}$$

Combine Eqs. (A16)-(19), we can get the linear equations as follow

$$\begin{bmatrix} W(1,1) & W(1,2) & W(1,3) & W(1,4) & W(1,5) & \cdots & W(1,50) & 1 \\ \cdots & \cdots & \cdots & \cdots & \cdots & \cdots & \cdots & 1 \\ W(50,1) & W(50,2) & W(50,3) & W(50,4) & W(50,5) & \cdots & W(50,50) & 1 \\ 1 & 1 & 1 & 1 & 1 & \cdots & 1 & 0 \end{bmatrix} \begin{bmatrix} \tilde{q}_{fD1} \\ \cdots \\ \tilde{q}_{fD50} \\ \tilde{p}_{wD} \end{bmatrix} = \begin{bmatrix} \frac{\pi x_{D1}}{sc_{fD}} \\ \cdots \\ \frac{\pi x_{D50}}{sc_{fD}} \\ \frac{1}{s\Delta x} \end{bmatrix} \tag{A20}$$

The wellbore pressure of a constant production hydraulic fracturing well in naturally fractured reservoirs is obtained after solving Eq. (A20) by using a Gaussian elimination approach.